2003

Spontaneous magnetization generated by spin, pulsating, and planar combustion synthesis

Karen S. Martirosyan
The University of Texas Rio Grande Valley

J. R. Claycomb

G. Gogoshin

R. A. Yarbrough

J. H. Miller Jr.

See next page for additional authors

Spontaneous magnetization generated by spin, pulsating, and planar combustion synthesis

K. S. Martirosyan
Department of Chemical Engineering, University of Houston, Houston, Texas 77204

J. R. Claycomb, G. Gogoshin, R. A. Yarbrough, and J. H. Miller, Jr.
Department of Physics and Texas Center for Superconductivity and Advanced Materials, University of Houston, Houston, Texas 77204

D. Luss[a)]
Department of Chemical Engineering, University of Houston, Houston, Texas 77204

(Received 14 November 2002; accepted 6 March 2003)

The motion of the high temperature front during combustion synthesis of ferrite materials generates residual magnetization in cylindrical product samples. The combustion wave created a current density of up to 10 A/cm^2, which influenced the magnetization distribution. The measured peak magnetic field intensity was up to 8 μT. Qualitatively different magnetic field maps were generated in ferrite samples synthesized by different combustion modes. The average magnetization vector generated by either planar or pulsating combustion was oriented at a smaller angle with respect to the pellet axis ($\phi \leqslant 45°$) than those generated by spin combustion ($60° \leqslant \phi \leqslant 80°$). We estimate that an internal transient magnetic field of up to 5 mT formed in the postcombustion region when its temperature was below the Curie temperature. This explains why the Earth's field had no impact on the spontaneous magnetization field. Model calculations reproduce the qualitative features of the measured field maps. © *2003 American Institute of Physics.* [DOI: 10.1063/1.1569997]

I. INTRODUCTION

Self-propagating high-temperature synthesis (SHS) is a method of producing ceramic materials by solid combustion.[1,2] Solid combustion may occur in several modes. During planar combustion, a planar reaction front propagates along the axis of the sample at a constant velocity. Self-oscillating or pulsating combustion is characterized by a planar front that propagates with fluctuating velocity. During spin combustion, localized hot spots spin in a spiral trajectory around the sample. The combustion front motion causes domain alignment and texturing of the synthesized materials. The combustion of ferrites generates spontaneous magnetization with residual magnetic fields of up to 10 μT.[3,4] The ignition location is close to the south magnetic pole irrespective of the orientation of the geomagnetic field. The absolute magnitude of the spontaneous magnetization of barium ferrite depended strongly on the phase structure (ferritizing degree) of the final products. Measurements using superconducting quantum interference devices showed that small, time dependent magnetic fields of about 20 nT were generated at a distance of about 20 mm from the sample during the solid combustion producing ferromagnetic ($BaFe_{12}O_{19}$, $NaFeO_2$, $LiFeO_2$) and paramagnetic or diamagnetic (TiO_2, ZrO_2, Cr_2O_3, etc.) materials.[5,6] Rapid magnetic field oscillations of up to ~100 Hz were observed during the synthesis of some oxides.[7] Potential differences of up to ~1.5 V were generated during solid combustion between two electrodes, inserted at a distance of about 5 mm.[8] The shape and magnitude of the temporal electric signal depended on the reactant properties, mode of combustion and mobility of the generated ions and cations.

At present, there are no established mechanisms explaining the generation of a transient electromagnetic field during solid combustion and the residual magnetization of the cooled products. Thus, the impact and potential applications of the generated magnetic field cannot be predicted. Information about the influence of the combustion mode on the spontaneous magnetization of ferrite products will enhance our understanding of the rate processes generating these electromagnetic fields and provide a critical test of any proposed mechanism.

This work is an experimental study of the nature and distribution of residual magnetization generated during combustion synthesis of several hard magnetic ferrites ($PbFe_{12}O_{19}$, $SrFe_{12}O_{19}$, $CoFeO_4$, $BaFe_{12}O_{19}$) and soft magnetic ferrites $CoFeO_4$, $Y_3Fe_5O_{12}$, $Li_{0.5}Fe_{2.5}O_2$). The ferrites are produced via the reaction:[9,10]

$$kn(2\mathrm{Fe}+1.5\mathrm{O}_2)+n(1-k)(\mathrm{Fe}_2^{3+}\mathrm{O}_3^{2-})+0.5m(\mathrm{Me}_2^{R}\mathrm{O}_R^{2-}) = (\mathrm{Me}_2^{R}\mathrm{O}_R^{2-})_{0.5m}(\mathrm{Fe}_2^{3+}\mathrm{O}_3^{2-})_n, \quad (1)$$

where Me is the metal characterizing the ferrite, m and n are integers, and k is a parameter that controls the exotermicity of the reaction. We investigated the influence of the combustion mode (planar, pulsating, and spin) on the distribution of the residual magnetization of the cooled products and determined the orientation and absolute magnitude of the internal magnetic fields generated during the combustion.

[a)]Author to whom correspondence should be addressed; electronic mail: dluss@uh.edu

II. EXPERIMENTAL PROCEDURE AND SETUP

The reactions were conducted in a quartz tube (10 cm inner diameter and 25 cm long) fed by oxygen at a flow rate of 1–5 l/m. To initiate a planar propagating front the samples were ignited by a ''chemical match'' ($Ti+BaO_2+0.5Al_2O_3$). The solid reactants were 99+% pure (Sigma-Aldrich Chemical Company) and were dried before the reaction for 5 h at 115 °C and then mixed for 4 h in a ball mill (US Stoneware, Mahwah, NY). Powder pressing was used to prepare cylindrical samples 12 mm in diameter, 30 mm long, with initial relative densities, (Δ), (ratio of sample density to that of a nonporous pellet) in the range of 0.5–0.7.

The combustion temperatures were measured with 0.1 mm diameter *S*-type (Pt–Rh) thermocouples inserted into the sample. The combustion front velocity was determined from the time that the temperature wave moved between two thermocouples separated by a distance of about 10 mm. The thermocouple and Pt-probe signals were recorded by a data acquisition system (Omega Eng. Inc. Stanford, CT) connected to a PC. The electrical current was measured between two Pt wires of $\varnothing=0.1$ mm separated by a distance of 5 mm. The impedance during voltage and current measurements were 0.25 MΩ and 0.1 Ω, respectively. The probe first exposed to the propagating front was connected to the negative lead of the ammeter.

The temperature front propagated from the top of the sample to its bottom. Increasing the initial density of the ferrite samples and/or decreasing the oxygen flow caused a transition of the combustion mode from planar to pulsating or spin. After combustion the samples were cooled down to room temperature. The residual magnetic fields were measured at various temperatures, from room temperature up to ~650 °C. This enabled determination of the Curie temperature (T_C) at which a ferromagnetic to paramagnetic phase transition occurs.

The products composition and phases were analyzed by x-ray diffraction (XRD) (Siemens D5000; Cu Kα radiation source). The diffraction lattice parameters were indexed by using either the TREOR or METRIC-LS program. Cross sections of the product samples were inspected by a microprobe (JEOL JAX8600, Japan) to determine their microstructure.

The magnetic measurements were carried out with the experimental setup shown in Fig. 1. The residual magnetic field of the products were measured by both planar and cylindrical scanning techniques. The sample was placed on a planar *X*–*Y* scanning table, driven by two independent stepper motors. The motion was computer controlled by a National Instruments general purpose interface bus interface with Labview software. The *Z*-component magnetic field intensity B_z of a product sample was detected with an Applied Physics Systems fluxgate magnetometer located above the sample. Data were simultaneously acquired with the Labview program after AD conversion and 5 Hz low pass filtering.

The cylindrical scanning technique measured the radial component of the magnetic field B_ρ over a cylindrical surface surrounding the sample. To enable controlled sample rotation, the motor belt was connected to a rotary rod with a sample holder at its end. The Maps of $B_\rho(\theta,Z)$ were recorded with the *Z* axis corresponding to the sample axis and θ varied between 0 and 2 π rad.

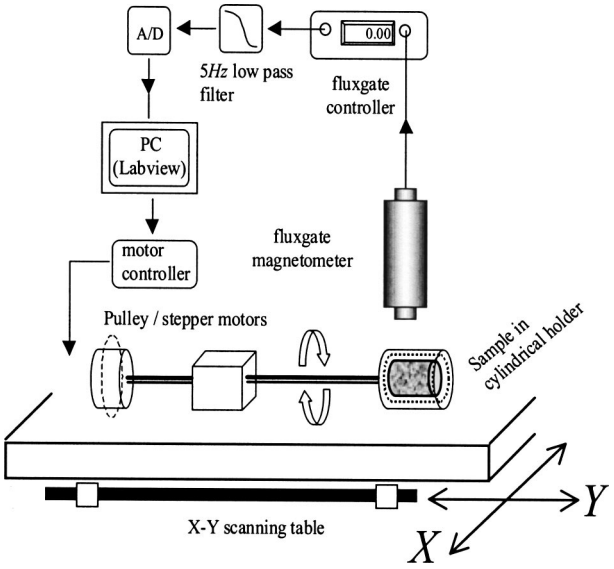

FIG. 1. Schematic of the experimental setup used for measuring the residual magnetic field distribution in cylindrical samples of ferrites made by SHS.

III. EXPERIMENTAL RESULTS

A. Sample preparation and current measurements

The combustion mode, temperature and moving front velocity depends on the physical structure (density, porosity, particle size, etc.) of the sample, its chemical composition and the ambient temperature. A transition from planar to either pulsating or spin combustion mode was obtained by increasing the sample relative density in the range of (0.5–0.7) and/or decreasing the oxygen flow rate in the range of 1–5 l/m. The initial iron powder mass was less than 25% to keep the combustion temperature between 900 and 1550 °C in order to prevent melting of the intermediate and/or the final products during the combustion.

A planar combustion with a front velocity of ~1.0 mm/s was obtained during the synthesis of strontium ferrite $SrFe_{12}O_{19}$ from a reactant mixture with Δ about 0.5 at an oxygen flow rate of 5 l/m. Increasing the initial relative sample density to 0.7 and reducing the oxygen flow rate to 1 l/m resulted in a spin combustion mode, in which a spot of about 1 mm diameter spinned in a helical trajectory around the sample surface at a velocity of about 0.4 mm/s with a pitch of about 2 mm. The combustion synthesis of cobalt and lead ferrite proceeded in a pulsating mode with an average planar front velocity of 0.8–1.2 mm/s. The pulsating front motion generated a product with a layered structure, each layer thickness was about 3 mm. The combustion caused less than 10% expansion of the sample length and diameter.

The maximal electrical current was generated when the samples temperature was between 750 and 1200 °C. Figure 2 shows the electrical current and temperature values during the combustion synthesis of strontium ferrite from a reactant mixture containing 20 wt. % Fe. The maximum current of 27

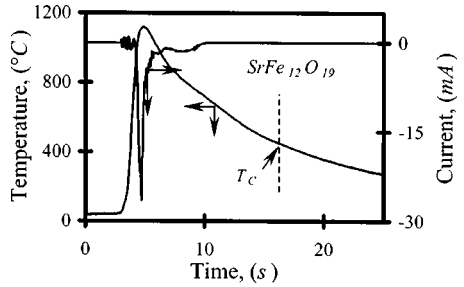

FIG. 2. Temporal temperature and current generated by the planar combustion mode of strontium ferrite, (T_C—Curie temperature).

mA was generated when the planar combustion front passed by the second electrode at a temperature of 850 °C. The electrical signal duration was 5.2 s, with a 2–5 mA current measured in the postcombustion zone. The sample cooled down from its maximum temperature of 1120 °C to the Curie temperature for strontium ferrite, ($T_C \sim 460$ °C) in about 11 s.

Table I reports the impact of the reactants composition, sample relative density, and oxygen flow rate on the maximum combustion temperature, electric current, and combustion mode during the combustion synthesis of several ferrites.

B. Microstructure and characteristics of final products

The yield of the desired ferrite in the product exceeded 80% in all the experiments. X-ray diffraction patterns show that the barium, strontium, and lead ferrite products had a hexagonal structure, the cobalt and lithium ferrite had a cubic spinel structure, and the yttrium ferrite had a garnet structure. The final product also contained intermediate nonmagnetic phases and an α modification of Fe_2O_3. Table II reports the lattice parameter of several product ferrites, as determined by XRD.

Figure 3 shows the microstructure in the center of strontium ferrite samples produced by planar and spin combustion. The photographs are of a cross section perpendicular to the axis of the sample. The average grain size produced by the planar and spin combustion is about 5–10 μm. The grains are distributed uniformly in both samples with the spin combustion product having a higher porosity.

TABLE II. X-ray diffraction lattice parameter values for ferrites produced by combustion synthesis.

Ferrite	Diffraction lattice parameter		Ferrite structure
	a (Å)	*b* (Å)	
$SrFe_{12}O_{19}$	5.86	23.06	
$BaFe_{12}O_{19}$	5.89	23.19	Hexagonal
$PbFe_{12}O_{19}$,	5.87	23.12	
$CoFeO_4$	8.38	···	
$Li_{0.5}Fe_{2.5}O_2$	8.34	···	Spinel
$Y_3Fe_5O_{12}$	12.37	···	Garnet

The dependence of the residual magnetic field of the product on the temperature was investigated by heating the products in a furnace and measuring the maximum remnant field with a fluxgate magnetometer. The experiments (Fig. 4) showed that the specific magnetization decreased with increasing temperatures between 450 and 650 °C. The magnetic field vanished above the Curie temperature.

C. Magnetic field mapping

The combustion mode affected the qualitative features of the magnetic field maps. Figure 5 describes the residual magnetic field in several ferrite product samples. The figure shows the X–Y spatial distribution of the z component of the magnetic field in the top, side, and bottom of some samples. The scanning area was 10×10 cm and the fluxgate was located 5 mm above the top of the pellet. The pellet was placed in a nonmagnetic sample holder under the magnetometer. X–Y scans of the top, side, and bottom of each sample were obtained by rotating the pellet sequentially by 90°. The maximum residual magnetic field of the various ferrites was between 0.1 and 8 μT.

Figures 5(a) and 5(b) are maps of the magnetic field formed in lithium and yttrium ferrite samples synthesized via spin combustion mode. When the magnetization is isotropic, its magnitude and direction are constant throughout the sample and rotating the pellet by 180° generates a ''mirror image.'' The top view of the Li-ferrite sample has a positive peak, $B_{max}=0.8$ μT while the bottom view has a negative peak $B_{min}=-1.1$ μT where the ratio $R=|B_{max}/B_{min}|=0.73$, while $R=1$ for uniform magnetization. The side view of the

TABLE I. Dependence of the combustion mode and maximum combustion current on the reactant mixture composition, sample density, and oxygen feed rate.

Ferrite	Contents of iron (%)	Initial relative density	Oxygen flow (l/m)	Combustion mode	Maximum combustion temperature, T_{max}, °C	Maximum current (mA)
$SrFe_{12}O_{19}$	20	0.5	5	Planar	1120	27
	20	0.7	1	Spin	1480[a]	18
$CoFeO_4$	25	0.6	4	Pulsating	900	26
$BaFe_{12}O_{19}$	22	0.5	5	Planar	1280	25
$Y_3Fe_5O_{12}$	20	0.62	3	Spin	1550[a]	26
$Li_{0.5}Fe_{2.5}O_2$	18	0.6	2	Spin	1430[a]	36
$PbFe_{12}O_{19}$	18	0.55	4	Pulsating	1000	35

[a]Temperature of moving hot spot on the surface.

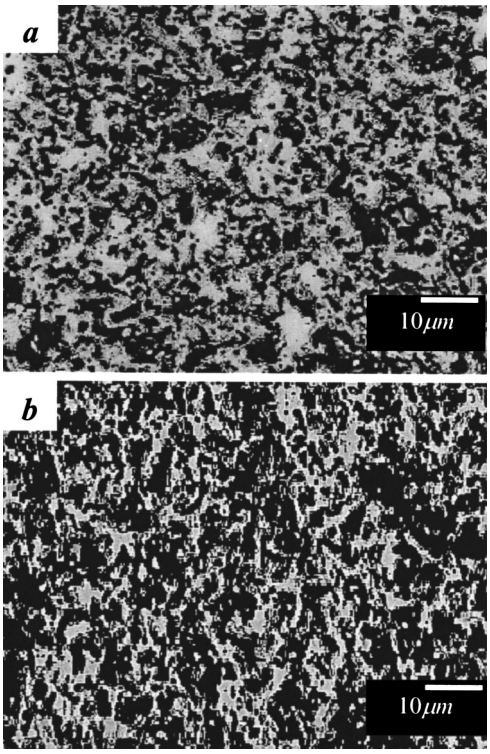

FIG. 3. Microsection of strontium ferrite on the sample center obtained by (a) planar and (b) spin combustion mode.

Li–ferrite pellet has both positive and negative peaks, indicating that the magnetization vector is nearly perpendicular to the combustion axis. The maps show that the maximum and minimum magnetic field lie roughly in a horizontal plane and that the average magnetization vector is nearly perpendicular to the pellet axis and is in the *y* direction. The degree of anisotropy can be estimated by comparing the top and bottom field maps obtained following a 180° rotation of the sample. The yttrium ferrite pellet also shows strong positive and negative peaks (R=0.81) in the bottom and top views with a slight distortion of the positive peak in the bottom. The side scan of the yttrium pellet reveals that the average magnetization vector is oriented at a large angle $\phi\sim70°$ with respect to the pellet axis but smaller than in the lithium pellet $\phi\sim80°$.

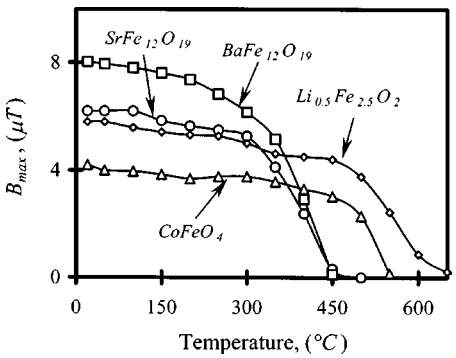

FIG. 4. Peak residual magnetic field of various ferrites recorded after heating postcombustion products.

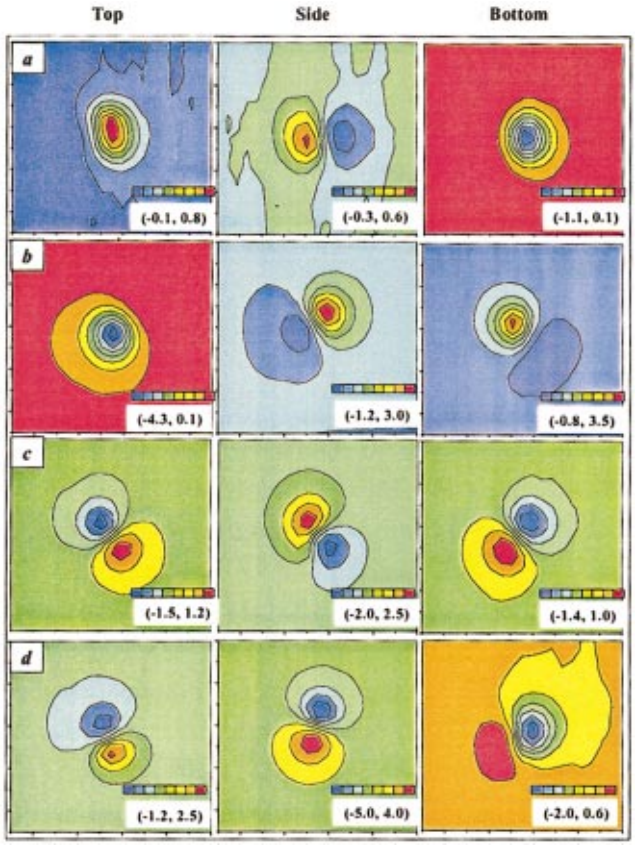

FIG. 5. (Color) Magnetic field maps of $Li_{0.5}Fe_{2.5}O_2$ (a), $Y_3Fe_5O_{12}$ (b) ferrite synthesized via spin combustion mode and $PbFe_{12}O_{19}$ (c), $BaFe_{12}O_{19}$ (d) ferrite synthesized via pulsating and planar combustion mode, respectively. Top, side, and bottom scans are made by 90° rotations of the pellet about its axis. The pellet is located at the center of each scan with the axis pointing toward the top of the page. Maximum (red) and minimum (blue) field values (in μT) are displayed in the lower right of each scan (distance between sample and sensor ~5 mm).

Figure 5(c) is the magnetic field maps of lead ferrite synthesized during a pulsating combustion mode. The field maps include both positive and negative peaks (R=0.86). The top and bottom scans appear to be mirror images, however, the side scan reveals a sign flip between the upper and lower peaks compared to the top and bottom scans. This indicates that the residual magnetization field varies throughout the sample. The magnetization vector is oriented at $\phi\sim45°$ with respect to pellet axis which is smaller than angles measured in spin combustion samples.

Field maps of a barium ferrite sample produced by a planar combustion [Fig. 5(d)] show that the magnetization vector is closer to the pellet axis ($\phi\sim20°$) than that in the samples produced by spin combustion. Strong anisotropy is evident from the asymmetry between the top and bottom scans of the Ba–ferrite sample (R=1.25). A high degree of anisotropy was also observed in the *X*–*Y* field maps of strontium (R=0.3) and cobalt ferrite (R=0.25) samples synthesized by planar combustion.

Magnetic field maps were also obtained using the cylindrical scanning technique, in which the radial component of the magnetic field B_ρ was measured over a cylindrical surface surrounding the pellet. The pellet was held parallel to

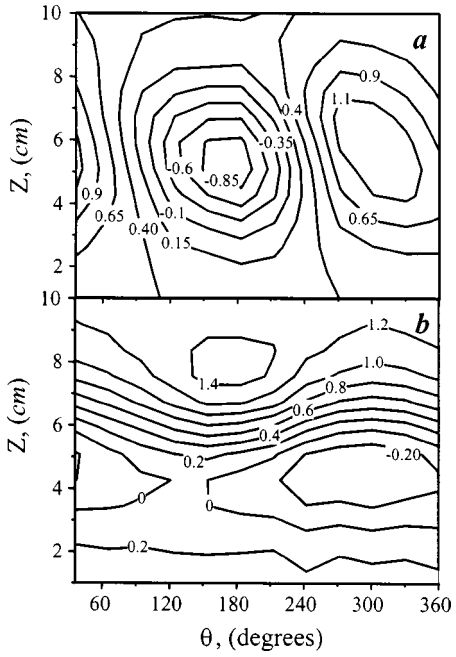

FIG. 6. Cylindrical distribution of the magnetic field, (in μT) resulting from (a) spin combustion and (b) planar combustion of strontium ferrite.

the vertical or z axis while the horizontal axis corresponds to the angle θ that the pellet was rotated during the scan. Figure 6 shows the cylindrical distribution of the residual magnetic field in a strontium ferrite sample produced by (a) spin combustion and (b) planar combustion. The field was periodic in θ, i.e., the contour lines on the left and right hand side of the figures are the same. The peak field positions in Fig. 6(a) indicate that the average magnetization vector is nearly perpendicular to the axis of the pellet, which is characteristic of spin combustion. The contour lines in Fig. 6(b) are more horizontal indicating that the pole positions are closer to the ends of the pellet. Magnetic dipole-like field distributions consisting of a positive and a negative peak were observed in all the $X-Y$ and $Z-\theta$ measurements of the ferrite compounds synthesized by different combustion modes. The south magnetic pole tended to be closer to the ignition point. We note that higher order multipole moments (quadrupole, octopole, etc.) are due to anisotropies in the magnetization distribution that distort the magnetic dipole field. However, the magnetic field contribution due to these higher order moments falls off as a l/d^n, where d is the distance between the dipole and field detector. For example, the field due to magnetic dipole and quadrupole moments falls off as $1/d^3$ and $1/d^5$, respectively. We now present a model predicting the radial cylindrical field distribution generated by a residual magnetization distribution in postcombustion products.

IV. MODEL OF A FIELD DUE TO A MAGNETIZATION DISTRIBUTION

We calculate the cylindrical magnetic field distribution of a cylindrical pellet with a uniform magnetization oriented at an angle ϕ with respect to the axis of the pellet. Figure 7 shows the cylindrical pellet of length $2h$ and radius a over

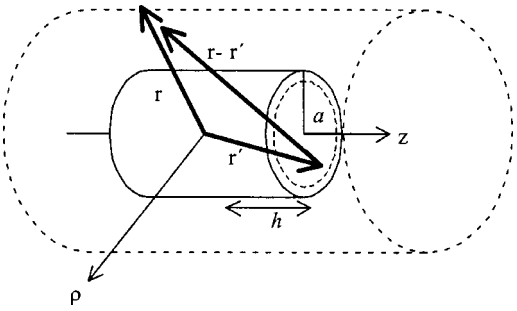

FIG. 7. The geometry of the cylindrical pellet and the surface over which the ρ component of magnetic field is measured. The pellet has a radius a and a length of 2 h. The sensor measures the field at a position r. The vector r' is swept over the surface of the pellet.

which the normal component of the surface magnetic field is measured. The magnetic field at a position $\mathbf{r}$ due to a magnetization distribution $\mathbf{M}$ is[11]

$$\mathbf{B}(\mathbf{r})=\frac{\mu_0}{4\pi}\int_{\mathrm{Vol}}\rho_M\frac{(\mathbf{r}-\mathbf{r}')}{|\mathbf{r}-\mathbf{r}'|^3}dV' + \frac{\mu_0}{4\pi}\int_{\mathrm{Surf}}\sigma_M\frac{(\mathbf{r}-\mathbf{r}')}{|\mathbf{r}-\mathbf{r}'|^3}da'+\mu_0\mathbf{M}(\mathbf{r}), \tag{2}$$

where $\mathbf{r}'$ and $\mathbf{r}$ are the source and field locations, dV' and da' correspond to the volume and surface elements of the pellet, respectively. The magnetic pole density in the volume of the sample is given by

$$\rho_M(\mathbf{r}')=-\nabla\cdot\mathbf{M}(\mathbf{r}') \tag{3}$$

and the surface density of the magnetic pole strength is

$$\sigma_M(\mathbf{r}')=\mathbf{M}(\mathbf{r}')\cdot\hat{\mathbf{n}}, \tag{4}$$

where $\hat{\mathbf{n}}$ is a unit vector perpendicular to the pellet surface. Since $\mathbf{M(r)}$ vanishes outside the sample, the third term in Eq. (2) vanishes for $\mathbf{r}>\mathbf{r}'$. When the magnetization is uniform, $M(r)$ is a constant, $\rho_M=0$, and only the second term in Eq. (2) contributes to the magnetic field distribution. If we take $\mathbf{M(r)}=M_x\mathbf{x}+M_z\mathbf{z}$ then the radial component of the magnetic field $B_\rho=\mathbf{B}\cdot\rho$, measured over a cylindrical surface of radius ρ, is

$$B_\rho=B_\rho^{\mathrm{side}}+B_\rho^{+}+B_\rho^{-}\,. \tag{5}$$

Here

$$B_\rho^{\mathrm{side}}(\theta,z)=\frac{\mu_0}{4\pi}\int_0^{2\pi}\int_{-h}^{h}\frac{M_x\cos(\theta')[\rho-a\cos(\theta'-\theta)]}{[\rho^2+a^2-2\rho a\cos(\theta'-\theta)+(z-z')^2]^{3/2}}\times a\,dz'\,d\theta' \tag{6}$$

and

$$B_\rho^{\pm}(\theta,z)=\frac{\mu_0}{4\pi}\int_0^{2\pi}\int_0^{a}\times\frac{\pm M_z[\rho-r'\cos(\theta'-\theta)]}{[\rho^2+r'^2-2\rho r'\cos(\theta'-\theta)+(z\mp h)^2]^{3/2}}\times r'\,dr'\,d\theta' \tag{7}$$

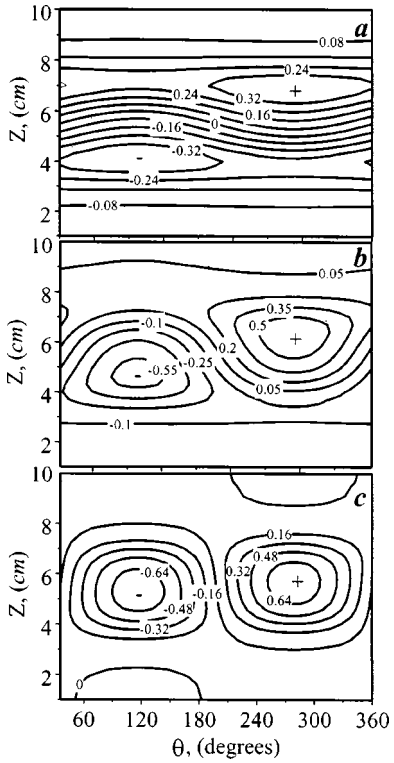

FIG. 8. Cylindrical field distribution (in units of 0.1 μT) of ferrite pellets with the angle ϕ between the magnetization vector and the z axis equal to (a) 10°, (b) 45°, and (c) 80°.

are the field contributions from σ_M on the cylindrical surface of the pellet and the end caps, respectively.

Figure 8 shows the calculated cylindrical field distribution for three isotropic magnetization distributions of pellets with an angle ϕ between the magnetization vector and the Z axis of (a) 10° (b) 45°, and (c) 80°. The peak field values in these figures are separated by $\Delta\theta=180°$ and $B_{\max}=-B_{\min}$. These predicted field distributions are qualitatively similar to those measured in the samples. We note that in general for anisotropic magnetization distributions, $\Delta\theta\neq180°$ and $R=|B_{\max}/B_{\min}|\neq1$. Thus, $\Delta\theta$ and R provide a measure of the anisotropy. Table III reports the R and $\Delta\theta$ values for several ferrite products synthesized by different combustion modes. For example for cobalt ferrite generated by oscillatory combustion $R=0.2$ and for yttrium ferrite generated by spin combustion $R=0.73$. The magnetic field was measured in 30° steps and a two-dimensional Lagrange interpolation function was used to estimate $\Delta\theta$.

TABLE III. Values of R and $\Delta\theta$ calculated from experimental data from different composition and combustion mode.

Sample	$R=\lvert B_{\max}/B_{\min}\rvert$	$\Delta\theta$ (degrees)	Combustion mode
$SrFe_{12}O_{19}$	0.76	154	Planar
	1.28	125	Spin
$CoFeO_4$	0.2	162	Pulsating
$Y_3Fe_5O_{12}$	0.73	162	Spin
$PbFe_{12}O_{19}$	1.16	154	Pulsating

V. DISCUSSION

The mode of the combustion synthesis affected the remnant magnetization distribution in various ferrite-based compounds. The magnetization vector of samples generated by spin combustion was roughly normal to the pellet axis, while planar combustion generated magnetization with poles located closer to the ends of the pellet. In all samples, the magnetic dipole moment was the dominant contribution to the total field, with the south magnetic pole close to the ignition point.

The magnetization vector may vary in magnitude and direction within the postcombustion product. This anisotropy generates higher order multipole moments that distort the dipole field. Sample anisotropy was gauged by the qualitative features of the X–Y magnetic field maps of pellets upon 90° and 180° rotations. The X–Y field maps provide a qualitative figure of merit for studying the anisotropic effect. The ratio of peak field intensities and the angle between the maximum and minimum field values were quantitative figures of merit obtained from cylindrical magnetic field maps.

Currently, no mechanism has been proposed that can relate the dynamics of the combustion mode in ferrite samples and the resulting magnetization distribution. We estimate here the field intensity formed in the sample during the combustion. The measured current density J in the combustion front is of the order of 10 A/cm^2. The field intensity inside the pellet during the combustion may be estimated by the Biot–Savart law

$$B=\frac{\mu}{4\pi}\int_{\substack{\text{comb.}\\ \text{wave}}}\frac{\mathbf{J}\times(\mathbf{r}-\mathbf{r}')}{|\mathbf{r}-\mathbf{r}'|^3}dV'\approx\frac{\mu}{4\pi}\frac{J(l\cdot A)}{\delta^2}. \tag{8}$$

The integral is over the volume of the combustion wave of length l, cross section area A, and a distance δ between the combustion wave and the sample region undergoing magnetic phase transition. δ depends on the combustion velocity and the time delay between the passing of the combustion front and the product cooling below the Curie temperature. For example, during the synthesis of strontium ferrite the time delay was ~11 s (Fig. 2) and the combustion velocity 0.1 cm/s, giving $\delta=1.1$ cm. This indicates that part of the sample cooled below T_C before the combustion front exited the sample. The permeability of ferrite samples is $\mu\sim\mu_0\times10^2$, (where μ_0—permeability of free space). Equation (8) predicts that in this case $B\sim5$ mT for δ of 1.1 cm. This value is about two orders of magnitude larger than the Earth's magnetic field. Thus, it is doubtful that Earth's field, which is on the order of 50 μT can cause significant field trapping. This conclusion is supported by the fact that experiments conducted in magnetically shielded enclosures generated residual magnetization even in this absence of the geomagnetic field.

The induced magnetization in cooled products may also generate fields that further induce magnetization in neighboring regions after the combustion wave passes through the sample. This may occur in a region of the sample cooled below the Curie temperature. The magnetic field in this region is due to currents flowing in the combustion zone and the remnant magnetization behind the critical region. A su-

perposition of magnetic fields in critical regions of the sample occurs as the products temperature decreases below T_C (450–650 °C). Figure 4 shows that the residual magnetization decreases with increasing temperature and vanishes near the Curie temperature.

The direction of the electric current coincides with the axis of the sample during the planar combustion of $SrFe_{12}O_{19}$ (Fig. 6). The poles of the corresponding magnetic field map were close to the ends of the pellet, at which the contours of constant B field were horizontal as the pellet is rotated around its axis. The vertical separation between the peak magnetic field values was 2.4 cm in Fig. 6(a). During spin combustion, the front propagated as a spot on a spiral with a ~2 mm pitch. The current basically flows in direction perpendicular to the axes of the sample. As shown in Fig. 6(b) contours of constant magnetic field are oriented along the axis of the sample between peak field values with vertical separation of 0.8 cm. The complex field maps are due to the spiral motion of the hot zone that generated the magnetization.

VI. CONCLUSIONS

The experiments reveal that the combustion mode affected the residual magnetization distribution in ferrite products. The average magnetization vector generated by planar and pulsating combustion were oriented at a smaller angle with respect to the z axis of the pellet than those generated by spin combustion. The combustion wave generated an electrical current which, in turn, produced an internal magnetic field. The magnetic field formed in part of the sample affected the orientation of the magnetization **M** within the other part of the sample after it cooled below the Curie temperature. We estimate from the measured current densities of order 10 A/cm^2 that the internal transient magnetic flux density during the combustion was about 5 mT, which is roughly two orders of magnitude greater than the geomagnetic field. Thus, the Earth's magnetic field does not significantly contribute to the residual magnetization. The absolute magnitudes of the spontaneous magnetization depend weakly on the material coercivity, while the distribution of residual magnetization depends strongly on the combustion mode. Model calculations were in qualitative agreement with experimentally measured magnetic field maps.

ACKNOWLEDGMENTS

The authors acknowledge the financial support by the NSF, the Materials Research Science and Engineering Center at the University of Houston, the Robert A. Welch Foundation (E-1221), the Texas Higher Education Coordinating Board Advanced Research and Technology Programs, the Texas Center for Superconductivity and Advanced Materials, and the Institute for Space Systems Operations.

[1] A. G. Merzhanov, in *Chemistry of Advanced Materials*, edited by C. N. R. Rao (Blackwell Scientific, Oxford, UK, 1992), p. 19.
[2] M. D. Nersesyan, P. B. Avakyan, K. S. Martirosyan, A. B. Komarov, and A. G. Merzhanov, Inorg. Mater. (Transl. of Neorg. Mater.) **29**, 1674 (1993).
[3] A. G. Merzhanov, S. O. Mkrtchyan, M. D. Nersesyan, P. B. Avakyan, and K. S. Martirosyan, Dokl. Akad. Nauk RA **93**, 81 (1992).
[4] P. B. Avakyan, M. D. Neresyan, and A. G. Merzhanov, Am. Ceram. Soc. Bull. **75**, 50 (1996).
[5] M. D. Nersesyan, J. R. Claycomb, Q. Ming, J. H. Miller, J. T. Richardson, and D. Luss, Appl. Phys. Lett. **75**, 1170 (1999).
[6] M. D. Nersesyan, J. R. Claycomb, J. T. Ritchie, J. H. Miller, J. T. Richardson, and D. Luss, J. Mater. Synth. Process. **9**, 63 (2001).
[7] M. D. Nersesyan, D. Luss, J. R. Claycomb, J. T. Ritchiea, and J. H. Miller, Jr., Combust. Sci. Technol. **169**, 89 (2001).
[8] M. D. Nersesyan, J. T. Ritchie, I. A. Filimonov, J. T. Richardson, and D. Luss, J. Electrochem. Soc. **149**, 11 (2002).
[9] K. S. Martirossian, P. B. Avakyan, and M. D. Nersesyan, Int. J. Self-Propagating High-Temp. Synth. **10**, 193 (2001).
[10] K. S. Martirosyan, P. B. Avakyan, and M. D. Nersesyan, Inorg. Mater. (Transl. of Neorg. Mater.) **138**, 400 (2002).
[11] J. R. Reitz, F. J. Milford, and R. W. Christy, *Foundations of Electromagnetic Theory,* 3rd ed. (Addison-Wesley, Reading, MA, 1980), p. 193.